Enhanced Dielectric Properties of Polyaniline Films with Manganese Dioxide and Zinc Oxide Nanorods in a Polyvinyl Alcohol (PVA) Matrix

Abdulwahhab H. Majeed[1], Leqaa A. Mohammed[1], Omar G. Hammoodi[1], Israa K.Mohammed[1], Tabark Ibrahem Kamel[1], Medea Ali Sultan[1], Sarah Zidane Khalaf [1], Zaid H. Mahmoud[1], Mustafa A. Alheety[2], M. Z. A. Yahya[3], I. M. Noor[4] and Pramod K. Singh[5]

[1]*Department of Chemistry, College of Science, University of Diyala, 32001 Baqubah, Iraq*

[2]*Department of Nursing, Al-Hadi University College, 10001 Baghdad, Iraq*

[3]*Faculty of Defence Science and Technology, Universiti Pertahanan Nasional Malaysia (UPNM), 57000 Kuala Lumpur, Malaysia*

[4]*Physics Division, Centre of Foundation Studies for Agricultural Sciences, Universiti Putra Malaysia, 43400 Serdang, Malaysia*

[5]*Center for Solar Cells and Renewable Energy, Department of Physics, School of Basic Sciences and Engineering, Sharda University, 201310 Greater Noida, India*

abdulwahhab@uodiyala.edu.iq, liqaaadnan@uodiyala.edu.iq, tabark93y@gmail.com, media98@gmail.com, nwnh01662@gmail.com, zaidhamid@uodiyala.edu.iq, mustafa1990alheety@gmail.com, mzay@upnm.edu.my, imnoor@upm.edu.my, pramodkumar.singh@sharda.ac.in, omerkazi@uodiyala.edu.iq, israak@uodiyala.edu.iq.

Keywords: MnO_2, ZnO, PANi, Nanocomposite and Dielectric Properties.

Abstract: In this study, polyaniline (PANI) was synthesized via oxidative polymerization, and nanoparticles of manganese oxide (MnO_2) and zinc oxide (ZnO) were prepared. The binary compounds, PANI-MnO2 and PANI-ZnO, were synthesized by in situ polymerization, where the oxides were mixed with aniline and polymerized in an ice bath using ammonium persulfate (APS) as the oxidizing agent. The resulting compounds were characterized using (FTIR, XRD and SEM). The polymer films were subsequently prepared, and the films containing polyvinyl alcohol (PVA) were characterized for their real and imaginary dielectric constants and electrical conductivity, using an LCR meter in order to measurement AC current. The PANI-MnO_2/PVA film exhibited highest intrinsic dielectric constant as compared to other specimens. The as-prepared PANI-ZnO/PVA film showed higher imaginary dielectric constant as compared to the original pure PVA film, indicating its better response to the variation of electric field. The PANI-ZnO/PVA film also stood first in the rank of the conductivity characteristics. Unlike pure PVA film, which showed unfavourable results in all these properties, the conductivity doping materials were absent in the control films.

1 INTRODUCTION

There is an important sub-class of organic materials, referred to as conducting polymers, with promise in a variety of emerging technologies including energy storage devices, electromagnetic interference shielding, electrochemical and biosensors, optoelectronic devices and many others [1]-[4]. These polymers have conjugated backbones, containing alternating single and double bonds which are necessary for the conduction of electricity. The oxidative polymerization reaction occurs on the side chain and results in the cleavage of some π bonds, and since free electrons make a material more conductive, this helps to increase the conductivity of the material as well [1]. The study of electron transport in these classes of polymers is particularly important because of their potential application in solid-state devices [2]. Polypyrrole, polythiophene, poly(3,4-ethylenedioxythiophene) and polyaniline (PANI) are examples of conducting polymers. Polymers of this kind are characterized by redox activity due to their content of heteroatoms and conjugated structures, providing a good basis for use in sensors and catalytic processes [3]. Polyaniline (PANI), among conductive polymers, has attracted a great deal of attention due to its special characteristics such as high conductivity,

unique conduction mechanism, ease of preparation, polymerization in bulk or on other materials, as well as good thermal stability and environmental benignity [4]. PANI is commonly used as a conductive mediator to improve electrical properties of semiconductor metal oxides by connecting their atoms [5]. Various approaches have employed integration with metal oxides, such as SnO_2, MnO_2 and ZnO, in order to enhance the electrical conductivity as well as performance of these hybrids [6]. Manganese dioxide (MnO_2) has attracted great interest from researchers because of its promising applications spanning a wide range of fields, including environmental remediation and energy management. MnO_2 is cost-effective and efficient in preparation, widely available so that it can be prepared in large quantities, as well as being relatively non-toxic. It exists in several crystalline forms, including α-, β-, γ-, δ-, and ε-types, with special note for its application in supercapacitors, various batteries, and sensors of all kinds. However, MnO_2 inherent low conductivity is a limitation that can be addressed by incorporating organic conducting matrices like conducting polymers [7]. Despite significant research on conducting polymers and their composites, studies focusing specifically on the AC conductivity of PANI/MnO_2 nanocomposites remain limited. Various preparation methods for PANI/MnO_2 nanocomposites are available, including chemical and electrochemical approaches [8]. On the other hand, because zinc oxide (ZnO) has important electrical characteristics and is n-type semiconducting, it is a metal oxide of significant importance. It is known for being affordable, cost-efficient, and offering strong mechanical, chemical, and environmental resilience. ZnO inherent photocatalytic abilities make it a valuable material; however, its wide band gap of 3.37 eV presents a barrier to its effectiveness in certain applications. In order to be genuinely beneficial, a photocatalyst must have the ability to break down many types of water contaminants, including heavy metals, dyes, and pharmaceutical residues, in addition to promoting the creation of hydrogen through water splitting [9]. To overcome ZnO limitations, integrating it into a polyaniline (PANI) matrix could be a promising strategy. This not only has the potential to enhance the composite's electrical conductivity but also to improve its sensitivity to visible light, thereby expanding its applications in photocatalytic processes. This approach holds promise for advancing environmental remediation technologies and promoting sustainable energy solutions [10]. Instead, to study electrical properties in terms of different types of materials, it is necessary to have a suitable mechanism for preparing polymeric compounds in the form of films, as most materials are in solid form and this effect cannot be studied directly for some electrical applications that need films or electrodes. A number of flexible polymers have been tried as matrix for solid materials, which lead to improved electrical properties. These polymers are poly(vinyl alcohol) (PVA), poly(vinyl chloride) (PVC), polystyrene (PS), polypropylene (PP), polyethylene (PE), and others [11]. PVA is one of the most common and widely used materials due to its low cost and ease of dissolving in water at moderate temperatures. It is non-toxic and environmentally friendly, with a good ability to store electrical charges. PVA also has high chemical, mechanical, and thermal stability, making it ideal for a wide range of applications, including synthetic medical devices, drug delivery systems, electrical and electronic devices, and energy storage devices, as well as many others [12].

In this study, nanoparticles of polyaniline, manganese oxide, and zinc oxide will be prepared. MnO_2-PANi and ZnO-PANI will also be prepared from these materials. Finally, various PVA films containing polyaniline, MnO_2-PANi, and ZnO-PANI will be prepared to study the effect of material changes on dielectric properties.

2 EXPERIMENTAL

2.1 Chemicals and Equipment

All solvents and chemicals were utilized just as they were, without any further purification. The research materials utilized in this study were procured from either Sigma-Aldrich, SDH, or Riedel-de hađn. A Perkin Elmer FT-IR 65 infrared spectrometer was used to record FTIR spectra. To evaluate the materials, a Philips/PW1730 XRD (Cu, Kα = 1.5406 Å) was also utilized. The size and shape of the produced nanomaterials were assessed using a scanning electron microscope (TESCAN, MAIA3). Finally, to study the electrical insulation properties, a device (GW INSTEK LCR-8105G) was used with a frequency range ranging from 20 kHz to 1000 kHz.

2.2 Procedure

2.2.1 Preparation of Polyaniline

To keep the temperature down, 10 mL of HCl (1 M) is mixed with 3 mL of aniline using an ice bath. 10

mL of 1 M HCl are used to dissolve two grams of ammonium persulfate (APS) in a different beaker. After that, the aniline solution is gradually mixed with the APS solution in a burette while being constantly stirred in the ice bath. Following the addition, the mixture is agitated in the ice bath for a further half hour, resulting in the formation of the dark green solution seen in Figure 1. The mixture is refrigerated for the whole night to allow it to polymerize. The next day, the product is rinsed several times with distilled water, filtered, and dried.

2.2.2 Preparation of MnO_2 NPs

To prepare MnO_2, a solution is first created by dissolving 3.68 g of $KMnO_4$ in 50 mL of distilled water. Simultaneously, another solution is prepared by dissolving 5.5 g of $MnSO_4$. $2H_2O$ in 50 mL of distilled water. Following the mixing of these two solutions, 1 mL of conc. HNO_3 will be added to the reaction container to bring the pH level closer to 1. After that, the reaction mixture is refluxed for 24 hours at 80°C. After the reaction, the residue is filtered and cleaned with distilled water until the pH approaches six, and the result is filtered again. Finally, the product is dried at a temperature at 110°C for 6 hours (seen in Figure 2) [13].

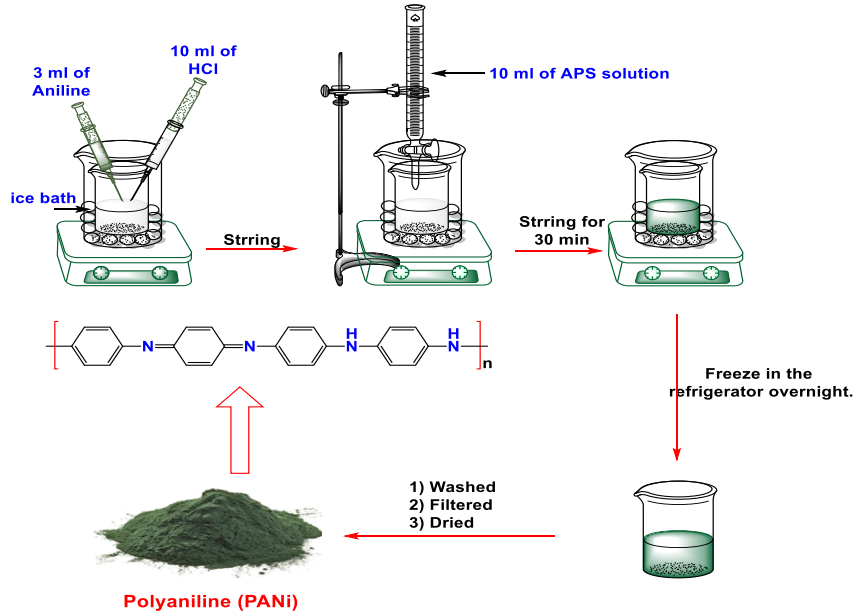

Figure 1: Schematic diagram of preparation of polyaniline.

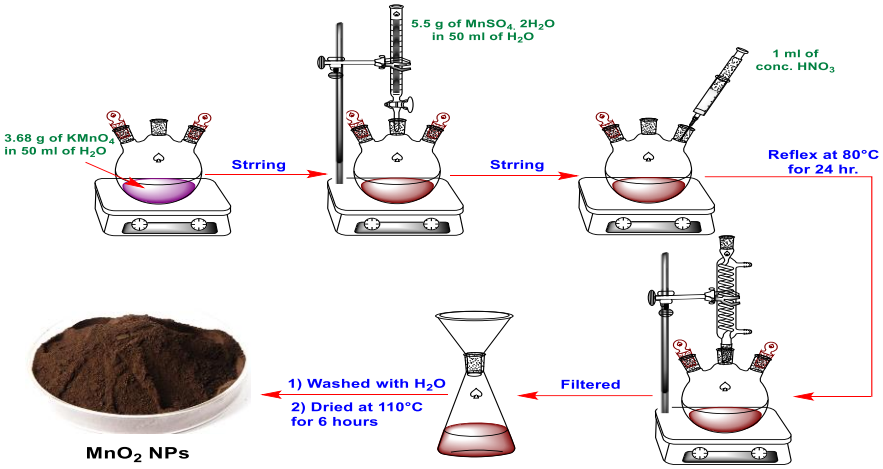

Figure 2: Schematic diagram of preparation of MnO2.

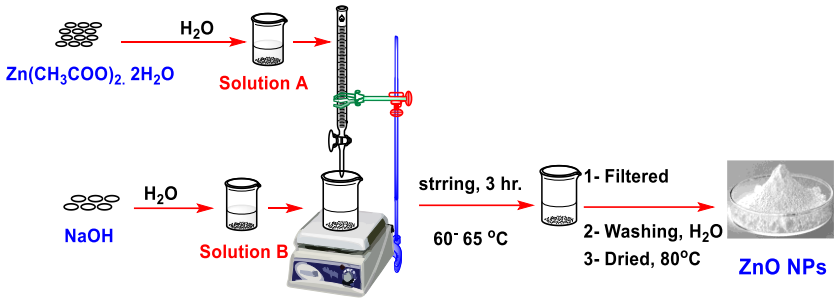

Figure 3: Schematic diagram of preparation of ZnO.

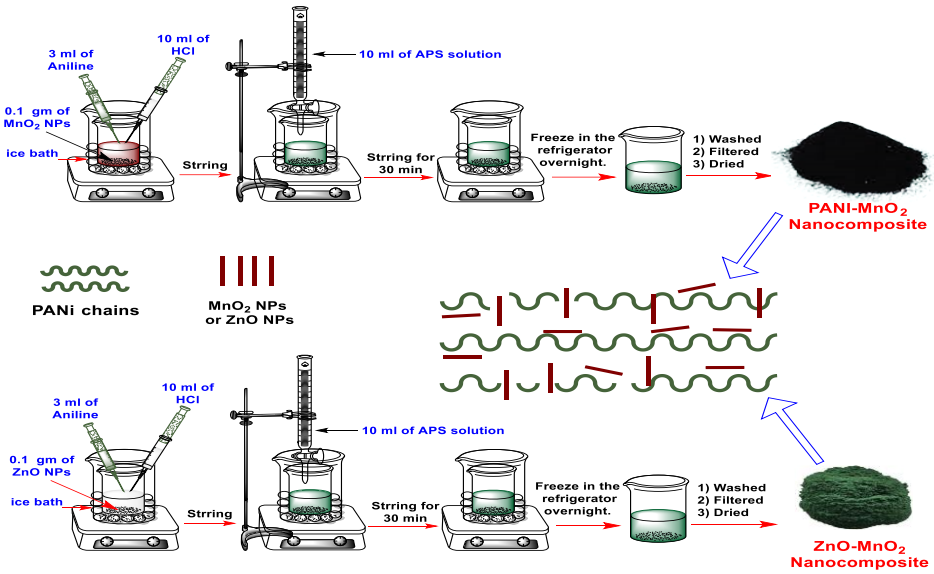

Figure 4: Schematic diagram of preparation of PANI-MnO2 and PANI-ZnO nanocomposites.

2.2.3 Preparation of ZnO NPs

The following technique is used to production ZnO: First, 2.2 g of $Zn(CH_3COO)_2.2H_2O$ are dissolved in 100 mL of distilled water while being constantly stirred until the dissolution is finished. 50 mL of distilled water are used to dissolve 0.8 g of NaOH to create a second solution. At a of 60–65°C, the first solution is then put in a burette and gradually added dropwise to the second solution while stirring quickly. After the addition is complete, the mixture is kept stirring at the same temperature for 3 hr. After that, the precipitate is filtered and repeatedly cleaned with distilled water until the pH is neutral. Lastly, the product is dried for 6 hr at 80°C (Fig. 3) [14].

2.2.4 Preparation of MnO2-PANI and ZnO-PANI Nanocomposites

To prepare the MnO_2-PANI nanocomposite, 0.1 g of MnO_2 is mixed with 3 mL of aniline. Then, 10 mL of 1 M HCl is added to the mixture, which is stirred continuously in an ice bath. Separately, 2 g of APS is dissolved in 10 mL of 1 M HCl. This APS solution is then placed in a burette and added dropwise to the MnO_2-aniline mixture under continuous stirring in the ice bath. After completing the addition, the mixture is stirred for an additional 30 min. in the ice bath before being transferred to a refrigerator and left overnight to allow polymerization to complete. The next day, the resulting product is washed several times with distilled water, filtered, and dried.

The same procedure is followed to prepare the ZnO-PANI nanocomposite, with ZnO replacing MnO_2 (Fig. 4).

2.2.5 Film Casting Method

1) Preparation of Poly (vinyl Alcohol) Solution (PVA Solution):
   - 5 g of PVA is dissolved in 100 mL of distilled water with continuous stirring at 60-70°C

until complete dissolution is achieved. The solution is then left overnight to ensure uniformity and to dissolve any remaining PVA crystals.

2) Preparation of the Films:

- 10 mL of the prepared PVA solution from the previous step is poured directly into a glass mold to prepare a pure PVA film.
- 0.1 g of the prepared polyaniline is weighed and mixed with 10 mL of the PVA solution prepared in the previous step. The mixture is homogenized using an ultrasonic device, then poured into a glass mold to prepare a polyaniline and polyvinyl alcohol film (PANI/PVA).
- 0.1 g of the prepared PANi-MnO2 nanocomposite is weighed and mixed with 10 mL of the PVA solution prepared in the previous step. The mixture is homogenized using an ultrasonic device, then poured into a glass mold to prepare a PANi-MnO2 nanocomposite and polyvinyl alcohol film (PANi-MnO2/PVA).
- 0.1 g of the prepared PANi-ZnO nanocomposite is weighed and mixed with 10 mL of the PVA solution prepared in the previous step. The mixture is homogenized using an ultrasonic device, then poured into a glass mold to prepare a PANi-ZnO nanocomposite and polyvinyl alcohol film (PANi-ZnO/PVA).

After two days, the films are removed from the glass molds and sent for electrical testing. Figure 5 illustrates the polymer film casting process [15], [16].

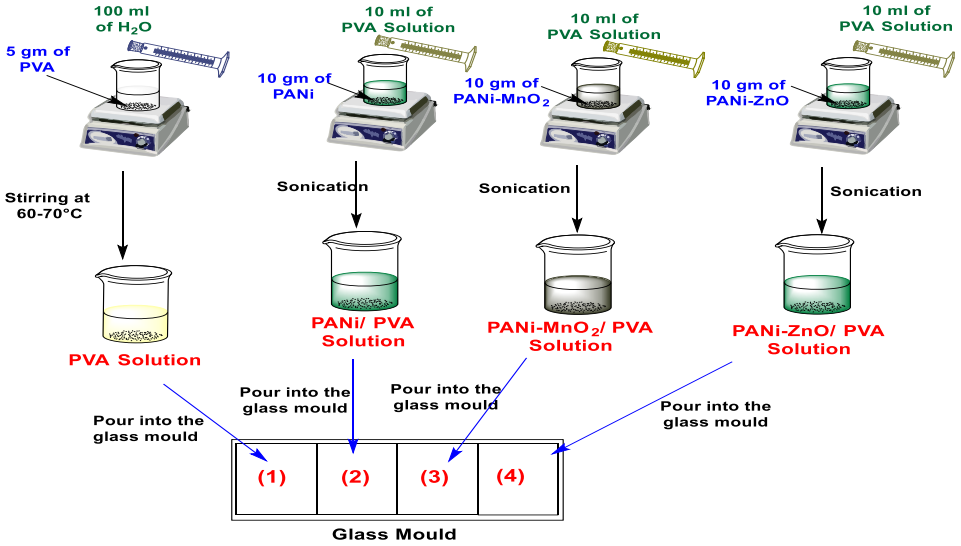

Figure 5: Schematic diagram of preparation of the polymeric films.

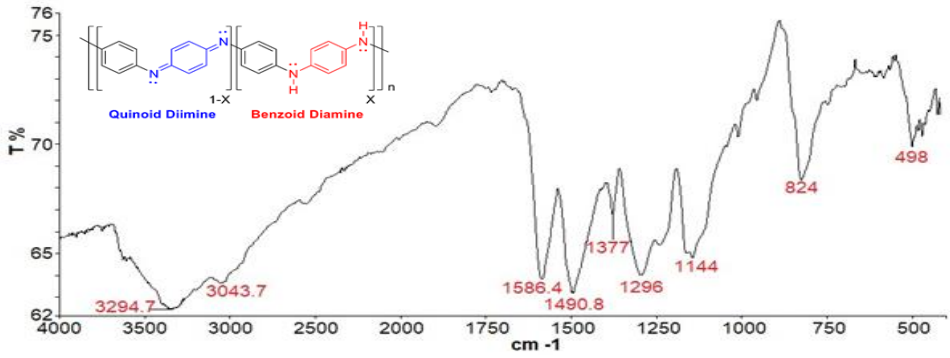

Figure 6: FTIR of polyaniline.

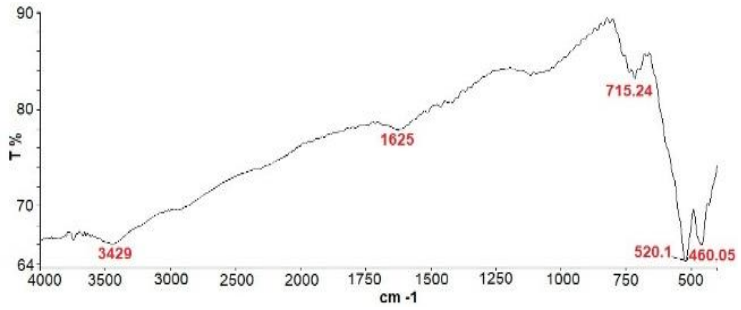

Figure 7: FTIR of manganese dioxide nanoparticles.

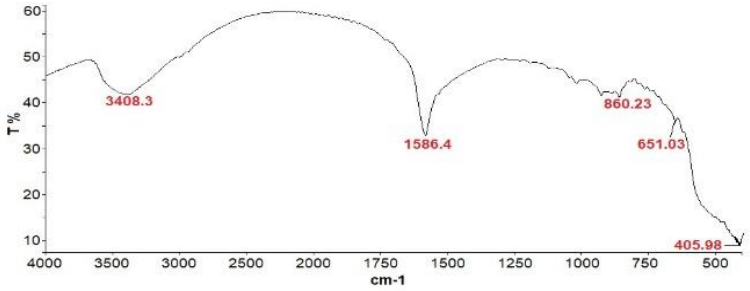

Figure 8: FTIR of zinc oxide nanoparticles.

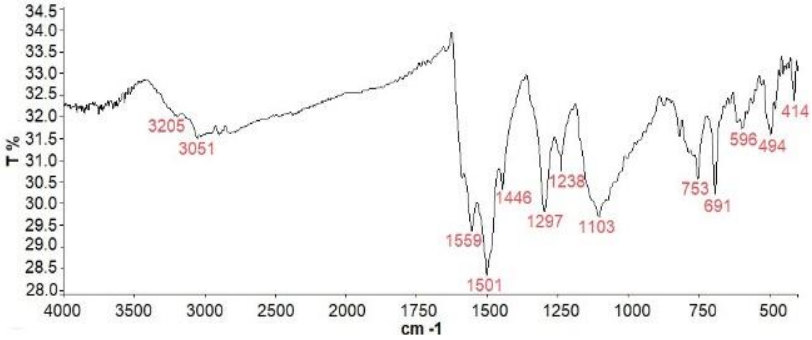

Figure 9: FTIR of PANI-MnO2 nanocomposite.

3 RESULTS AND DISCUSSIONS

3.1 FTIR of Polyaniline (PAni)

Figure 6 displays the FTIR spectrum of pure polyaniline (PAni). The amine group's stretching vibrations are responsible for the peak at 3294 cm^{-1}, whereas the amine group's bending vibrations in the quinoid and benzenoid rings of polyaniline are linked to the peaks at 1577 and 1495 cm^{-1}, respectively. Moreover, at 1135 cm^{-1} we find the typical absorption of N=Q=N, and at 1297 cm^{-1} we observe the stretching vibration of C-N. However, the aromatic ring's C-H bond is thought to be responsible for the band at 3043 cm^{-1} [17].

3.2 FTIR of MnO2 Nanoparticles

Figure 7 shows the FTIR spectrum of nano manganese dioxide within the range of 400-800 cm^{-1}. The O-Mn-O vibrations of the manganese dioxide nanostructure are responsible for the peaks in this spectrum located at 715, 520, and 463 cm^{-1}. Because of the large surface area of the MnO_2 nanostructure, the peaks at 3446 and 1624 cm^{-1} correspond to the stretching and bending vibrations of the hydroxyl group (-OH) caused by the presence of water molecules between the manganese dioxide nanoparticles [18].

3.3 FTIR of ZnO Nanoparticles

The prepared zinc oxide (ZnO) nanoparticles' FTIR spectra is seen in Figure 8. There is a noticeable wide peak at 3408 cm^{-1}, which is associated with the stretching vibrations of the hydroxyl group (-OH) from the water molecules that are in between the zinc oxide nanoparticles. The hydroxyl group (-OH) bending vibrations of water molecules are responsible for another peak at 1630 cm^{-1}. The presence of Zn-O in zinc oxide is responsible for the peaks seen at 405 and 651 cm^{-1} [19].

3.4 FTIR of PANI-MnO2 Nanocomposite:

Figure 9 illustrations the FTIR spectrum of the PANI-MnO2 nanocomposite. Multiple peaks are observed across the spectrum range of 400-4000 cm^{-1}. The peaks at 3205, 3051, 1559, 1501, 1446, 1297, and 1103 $cm^{-1}$are attributed to polyaniline, as previously explained in Figure 4. The peaks at 414, 596, and 691 $cm^{-1}$are associated with the manganese dioxide nanostructure, as shown in Figure 9. The presence of manganese dioxide peaks along with polyaniline in this spectrum indicates the successful in-situ polymerization between polyaniline and manganese dioxide nanoparticles [20].

3.5 FTIR of PANI-ZnO Nanocomposite

Figure 10 shows the FTIR spectrum of the PANI-ZnO nanocomposite. Multiple peaks are observed across the spectrum range of 400-4000 cm^{-1}. The peaks at 3234, 3084, 1583, 1551, 1480, 1294, and 1147 cm^{-1} are attributed to polyaniline, as previously explained in Figure 4. The peaks at 500 and 693 cm^{-1} are associated with the zinc oxide nanostructure, as shown in Figure 8. The peak at 3485 cm^{-1} is due to the presence of some water molecules in the composite. The presence of zinc oxide peaks along with polyaniline in this spectrum indicates the successful in-situ polymerization between polyaniline and zinc oxide nanoparticles [21].

3.6 XRD of MnO2 Nanoparticles:

Figure 11 shows the X-ray diffraction (XRD) analysis of nanostructured manganese oxide. Several peaks are observed at 2θ = 12.6734°, 18.0281°, 28.6951°, 37.5307°, 41.8776°, 49.6584°, 55.8058°, 60.0293°, 65.3576°, 69.1015°, and 72.9604°. This analysis's diffraction peaks all match the pure α-MnO_2 phase, which is consistent with JCPDS card No. 44-0141 [22]. The particle size of manganese oxide nanoparticles, according to the Debye-Scherrer equation, was found to be 16.82 nm. The great purity of the synthesized product was shown by the absence of peaks from other phases.

3.7 XRD of Zinc Oxide (ZnO) Nanoparticles

On the other hand, the X-ray diffraction (XRD) analysis of zinc oxide nanoparticles shows several sharp and pure peaks, as illustrated in Figure 12. These peaks are observed at 2θ = 31.7189°, 34.3224°, 36.2830°, 47.6227°, 56.5642°, 62.9247°, 66.4878°, 68.0870°, 69.1588°, 72.7933°, and 77.1045°. These findings align with other previously published research as well as the standard card for zinc oxide (JCPDS Card No. 36–1451). The particle size of the zinc oxide nanoparticles, according to the Debye-Scherrer equation, was found to be 17.38 nm. Since there are no peaks from other phases in the analyzed spectrum, the produced zinc oxide is thus regarded as being extremely pure [23].

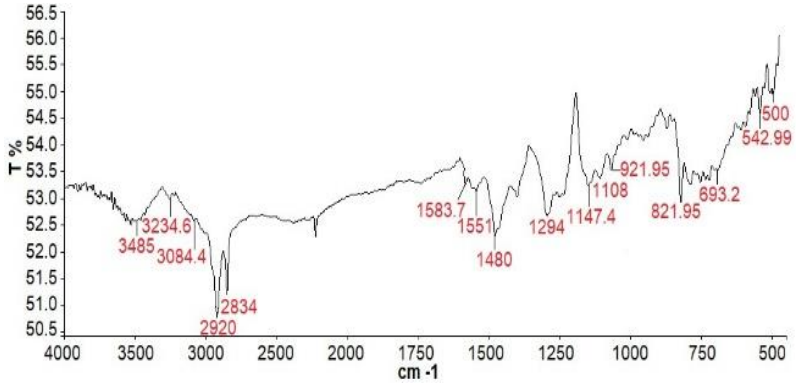

Figure 10: FTIR of the PANI-ZnO nanocomposite.

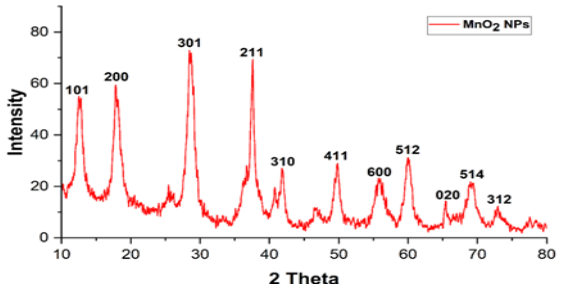

Figure 11: XRD of manganese oxide nanoparticles.

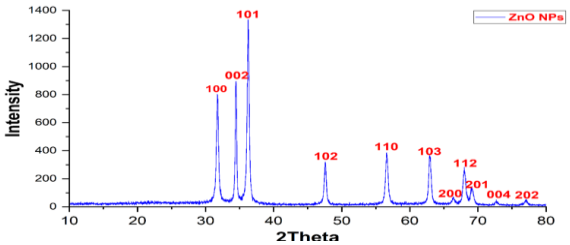

Figure 12: X-ray diffraction of nano zinc oxide.

3.8 SEM of MnO2 NPs

A scanning electron microscope (SEM) was used to examine the surface characteristics of the produced materials and the molecular sizes of the generated oxides. Manganese oxide nanorods made in the form of various lengths and diameters ranging from (14-34 nm) are seen in Figure 13 and were prepared using the previously described approach. These shapes have a distinctive effect on displaying the electrical properties of these materials, because the good and ordered alignment of the compound improves the electrical properties and reduces the percentage of energy lost due to distortion [15].

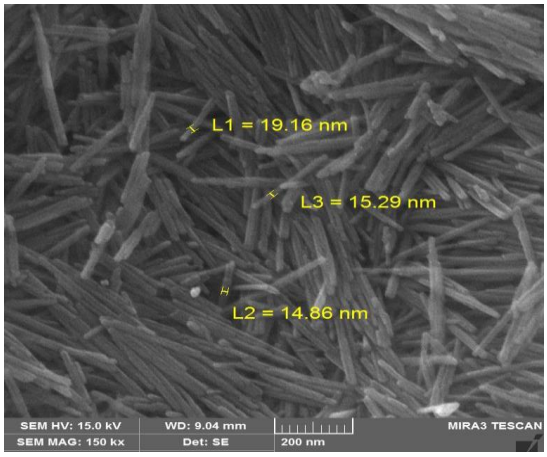

Figure 13: SEM of MnO2 nanorods.

3.9 SEM of ZnO NPs

On the other hand, SEM measurement was used also to study the morphology of the prepared zinc oxide. Zinc oxide (ZnO) nanorods, shown in Figure 14, exhibit a characteristic rod-like structure, with diameters between 40 and 65 nm. SEM images provide a clear visualization of these nanotubes, highlighting their beautiful elongated shape which often has a significant impact on the electrical properties of this compound.

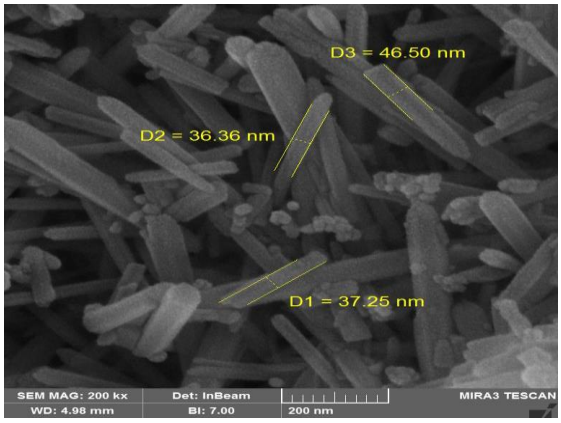

Figure 14: SEM of ZnO nanorods.

3.10 The Electrical Properties

The electrical properties of the polymer nanocomposites, including real and imaginary permittivity and electrical conductivity, were measured using an LCR meter. Measurements were conducted at frequencies ranging from 20 kHz to 1000 kHz and at room temperature [24].

Real Permittivity (ε'). Real permittivity describes the ability of materials to store energy when exposed to an electric field and is calculated using the following equation:

$$\varepsilon' = C.d/\varepsilon^{\circ}A, \quad (1)$$

where:

- C= capacitance;
- A = area of the electrode, which is 1 cm²;
- d = thickness of the film;
- εo = permittivity of free space, with a constant value of 8.85×10-12 F/m.

3.11 Imaginary Permittivity (Ɛ")

Imaginary permittivity represents the amount of electrical energy that is converted into thermal energy over time. It is a poor measure for materials used in

electrical storage, as a higher value indicates poorer energy storage capability. The tangent of the loss angle (tanδ) can be extracted from the ratio of imaginary to real permittivity:

$$\tan \delta = \varepsilon''/\varepsilon'. \quad (2)$$

Rearranging (2) gives:

$$\varepsilon'' = \tan\delta.\ \varepsilon', \quad (3)$$

$$\varepsilon'' = D.\ \varepsilon'. \quad (4)$$

The value of tanδ can be substituted with a constant denoted as D, known as the loss factor or dissipation factor:

$$\varepsilon'' = D.\ \varepsilon', \quad (5)$$

where:

- ε'' = imaginary permittivity;
- D = loss factor;
- ε' = real permittivity.

Figures 15 and 16 show the relationship between real and imaginary permittivity with the logarithm of frequency for the polymer nanocomposite films. It is observed that the real permittivity of all polymer composites reaches its highest value at the lowest frequency, as shown in Figure 15, and then gradually decreases with increasing frequency, reaching its lowest value at high frequencies. This can be explained by the fact that at low frequencies, the field oscillation is slow enough to allow permanent and induced dipoles to align with the applied field, while at high frequencies, the time period is shorter than the time needed for the molecules to align with the external electric field, leading to lower permittivity [24], [25]. Additionally, it is noted that the film composed of PANi-MnO_2/PVA exhibits the highest real permittivity, indicating it is the best at storing electrical energy, followed by PANi-ZnO/PVA, then the film containing polyaniline PANi/PVA, and finally, the Pure PVA film. This analysis suggests that doping PVA with polyaniline and its derivatives enhances the electrical properties of this polymer.

However, the imaginary permittivity Figure 16, calculated from the (4), shown similar behavior for the composites turned up. At low frequencies, the value of imaginary permittivity is substantial and decreases gently with increasing frequency. The imaginary permittivity with enhanced concentration is caused by the elevated conductive fillers lying in more conductive paths that result in greater current slipping and lower electrical insulation [25]. As seen in this figure are the PANi-ZnO/PVA with highest imaginary permittivity suggesting that the highest energy loss occurs in PANi-ZnO/PVA film, followed by PANi-MnO_2/PVA film, followed by film of polyaniline PANi/PVA and that of Pure PVA, suggesting that the energy dissipation would be least taking it as the basis.

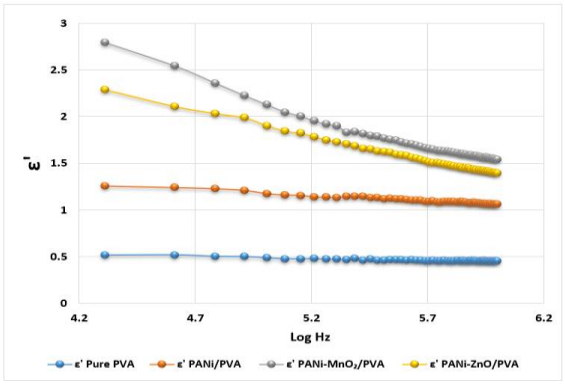

Figure 15: Relationship between real permittivity and logarithm of frequency for polymer nanocomposites.

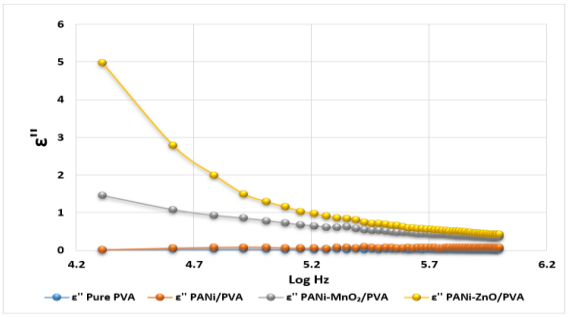

Figure 16: Relationship between imaginary permittivity and logarithm of frequency for polymer nanocomposites.

3.12 Electrical Conductivity (σ)

Electrical conductivity can be defined as the process of charge transfer from one place to another in a medium when an electric field is applied [24], [25].

The electrical conductivity values of the nanocomposites were studied using alternating current at various frequencies ranging from 20 kHz to 1000 kHz and at room temperature. The values were calculated using the following equations:

$$\sigma_{a.c} = \omega\ \varepsilon^{\circ}\varepsilon'\ \tan\delta. \quad (6)$$

ω=2πf, ε''= tanδ ε', sub (ω) and (Ɛ") in (6) yield:

$$\sigma_{a.c} = 2\pi f\ \varepsilon^{\circ}\varepsilon'', \quad (7)$$

where:

- σ : electrical conductivity;
- ω= The angular frequency;
- f= frequency used in measurements.

Electrical conductivity is the process of charge transfer from one place to another through a medium when an electric field is applied. The electrical conductivity of the polymer nanocomposites was measured, showing that the alternating current conductivity increases with frequency at room temperature, as illustrated in Figure 17. It is also observed that as the amount of filler (doped material) in the film increases, the electrical conductivity increases. This is logical because a higher amount of conductive filler increases the number of charge carriers, thus improving the film's electrical conductivity. Consequently, the Pure PVA film does not exhibit electrical conductivity even at high frequencies and is considered an insulator due to the lack of charge carriers that enhance electrical conductivity [26] - [30]. The figure shows that the best film with alternating current conductivity is PANi-ZnO/PVA, followed by PANi-MnO_2/PVA, then the film containing polyaniline PANi/PVA, and finally, the Pure PVA film.

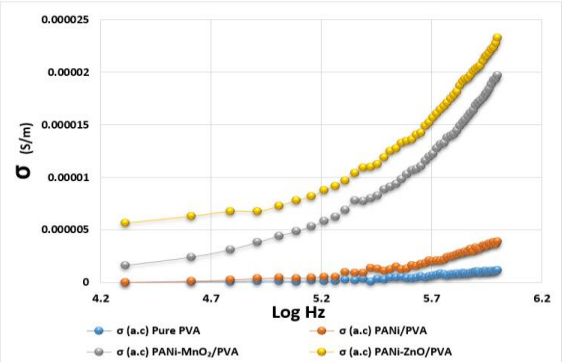

Figure 17: Relationship between electrical conductivity and logarithm of frequency.

In summary, Table 1 provides a comprehensive overview of the real and imaginary permittivity values, as well as the AC electrical conductivity, measured at both the highest and lowest frequencies for the as-prepared films. These data provide important insights into the dielectric behavior and conductivity of films across the frequency spectrum that have been demonstrated previously. By comparing these values, one can observe how the incorporation of different materials, such as MnO_2 and ZnO, into the PANI matrix affects the electrical properties of the composite films. The differences in permittivity and conductivity across different frequencies underscore the potential applications of these materials in fields where frequency-dependent dielectric and conductive properties are crucial, such as in capacitors, sensors and other electronic devices.

Table 1: Values of real and imaginary permittivity and AC electrical conductivity at the highest and lowest frequency for the prepared films.

Films	*f* (kHz)	ε'	ε''	σ (a.c) S/m
Pure PVA	20	0.5127	0.0148	1.68E-08
	1000	0.449	0.0214	1.1E-06
PANi/PVA	20	1.253	0.0146	1.67E-08
	1000	1.059	0.0701	3.8E-06
PANi-MnO_2 /PVA	20	2.793	1.4477	1.65E-06
	1000	1.541	0.3543	0.000019
PANi-ZnO/PVA	20	2.287	4.9651	5.65E-06
	1000	1.395	0.4184	0.000023

4 CONCLUSIONS

In conclusion, the study successfully achieved the synthesis of polyaniline (PANI) through oxidative polymerization, alongside the preparation of MnO_2 and ZnO nanoparticles, each exhibiting distinct morphological and structural features. By employing an in situ polymerization approach, binary nanocomposites of PANI–MnO_2 and PANI–ZnO were effectively developed, ensuring uniform distribution of the metal oxide nanoparticles within the polymer matrix. Structural characterization via X-ray diffraction (XRD) validated the crystalline behavior and phase purity of the synthesized materials, while scanning electron microscopy (SEM) revealed the formation of well-defined nanorods in the metal oxide structures, confirming successful synthesis at the nanoscale.

To further evaluate their functional capabilities, the prepared nanocomposites were incorporated into polyvinyl alcohol (PVA) to fabricate polymeric films with enhanced electrical performance. The introduction of the PANI-based composites into the PVA matrix resulted in substantial improvements in electrical properties compared to pure PVA, which inherently lacks mobile charge carriers and therefore exhibits minimal conductivity. The PANI–MnO_2/PVA composite film demonstrated the highest intrinsic dielectric constant, highlighting its strong potential for use in dielectric and energy-storage applications. Conversely, the PANI–ZnO/PVA film outperformed others in terms of electrical conductivity, indicating its suitability for conductive polymer applications such as flexible electronics, sensors, and charge-transport devices.

Overall, the findings demonstrate that integrating metal oxide nanoparticles with conducting polymers like PANI can significantly enhance the electrical

behavior of polymer-based materials. The improved dielectric and conductive characteristics of the composite films underscore their promise for a wide range of advanced electronic, optoelectronic, and energy-related applications, paving the way for further optimization and development of multifunctional conductive polymer nanocomposites.

REFERENCES

[1] S. Chen et al., "Asymmetric alicyclic amine-polyether amine molecular chain structure for improved energy storage density of high-temperature crosslinked polymer capacitor," Chemical Engineering Journal, vol. 387, p. 123662, May 2020.

[2] A. Feng, M. Ma, Z. Jia, M. Zhang, and G. Wu, "Fabrication of NiFe2O4@carbon fiber coated with phytic acid-doped polyaniline composite and its application as an electromagnetic wave absorber," RSC Advances, vol. 9, no. 44, pp. 25932-25941, Jan. 2019.

[3] Z. Jia et al., "Development of spindle-cone shaped of Fe/α-Fe2O3 hybrids and their superior wideband electromagnetic absorption performance," Journal of Alloys and Compounds, vol. 799, pp. 216-223, May 2019.

[4] Z. H. Mahmoud, J. M. Mahmood, N. S. Al-Obaidi, and A. M. Rahima, "Gama-Fe2O3 silica-coated 2-(2-benzothiazolyl azo)-4-methoxyaniline for supercapacitive performance," Journal of Electrochemical Science and Engineering, Feb. 2023.

[5] R. E. John, A. Chandran, M. Samuel, M. Thomas, and K. C. George, "Origin of colossal dielectric behavior in hydrothermally prepared non-stoichiometric α-MnO2 nanorods," Physica E: Low-dimensional Systems and Nanostructures, vol. 116, p. 113720, Feb. 2020.

[6] S. Palsaniya, H. B. Nemade, and A. K. Dasmahapatra, "Graphene based PANI/MnO2 nanocomposites with enhanced dielectric properties for high energy density materials," Carbon, vol. 150, pp. 179-190, Sep. 2019.

[7] S. Shivakumara, T. R. Penki, and N. Munichandraiah, "Preparation and electrochemical performance of porous hematite (α-Fe2O3) nanostructures as supercapacitor electrode material," Journal of Solid State Electrochemistry, vol. 18, no. 4, pp. 1057-1066, Dec. 2013.

[8] S. Shivakumara and N. Munichandraiah, "In-situ preparation of nanostructured α-MnO2/polypyrrole hybrid composite electrode materials for high performance supercapacitor," Journal of Alloys and Compounds, vol. 787, pp. 1044-1050, May 2019.

[9] M. Ganeshbabu, N. Kannan, P. S. Venkatesh, G. Paulraj, K. Jeganathan, and D. MubarakAli, "Synthesis and characterization of BiVO4 nanoparticles for environmental applications," RSC Advances, vol. 10, no. 31, pp. 18315-18322, 2020.

[10] S. Vijayalakshmi, E. Kumar, P. S. Venkatesh, and A. Raja, "Preparation of zirconium oxide with polyaniline nanocatalyst for the decomposition of pharmaceutical industrial wastewater," Ionics, vol. 26, no. 3, pp. 1507-1513, Nov. 2019.

[11] P. L. Reddy et al., "Dielectric properties of polyvinyl alcohol (PVA) nanocomposites filled with green synthesized zinc sulphide (ZnS) nanoparticles," Journal of Materials Science: Materials in Electronics, vol. 30, no. 5, pp. 4676-4687, Feb. 2019.

[12] S. Xi, X. Qian, X. Cheng, H. Liu, H. Shabanzadeh, and D. Dastan, "One-step depositing method of PAni/MnO2 composites for enhanced supercapacitor performance," iScience, vol. 28, no. 2, pp. 111774-111774, Jan. 2025.

[13] N. S. Al-Obaidi, Z. S. Al-Garawi, and A. S. Al-Mahdawi, "Polyaniline doping with nanoparticles: A review on the potential of electrical properties," Journal of Physics Conference Series, vol. 1853, no. 1, pp. 012055-012055, Mar. 2021.

[14] H. M. Ragab et al., "Tailoring optical and electrical properties of hybrid polymer nanodielectrics: Synthesis and characterization of CuO/TiO2 nanoparticle-embedded HPMC/NaAlg blend," Ceramics International, vol. 51, no. 13, pp. 17302-17310, Jan. 2025.

[15] A. H. Majeed, T. Bakir, and D. H. Hussain, "Dielectric properties of synthesized ternary hybrid nanocomposite embedded in poly (vinyl alcohol) matrix films," Polymers and Polymer Composites, vol. 29, no. 7, pp. 1089-1100, Aug. 2020.

[16] L. A. Mohammed et al., "Design and characterization of novel ternary nanocomposite (rGO-MnO2-PoPDA) product and screening its dielectric properties," International Journal on Interactive Design and Manufacturing (IJIDeM), vol. 17, no. 5, pp. 2387-2401, Aug. 2022.

[17] P. Mohapatra et al., "Synergistic effect of silver nanoparticles decorated graphene quantum dots nanohybrids reinforced polyaniline ternary nanocomposites on optical, thermal, and dielectric properties," Composite Interfaces, pp. 1-26, Jul. 2024.

[18] A. I. Al-Sulami et al., "Structural, optical, and electrical properties of Bi2O3/MWCNT-doped PVA/NaAlg nanocomposite films for flexible electronic applications," Journal of Science: Advanced Materials and Devices, vol. 10, no. 4, p. 100979, Sep. 2025.

[19] U. Acar Çevik, B. N. Sağlık, B. Korkut, Y. Özkay, and S. Ilgın, "Antiproliferative, cytotoxic, and apoptotic effects of new benzimidazole derivatives bearing hydrazone moiety," Journal of Heterocyclic Chemistry, vol. 55, no. 1, pp. 138-148, Oct. 2017.

[20] W. Kai, "Electrodeposition synthesis of PANI/MnO2/graphene composite materials and its electrochemical performance," International Journal of Electrochemical Science, pp. 8306-8314, Sep. 2017.

[21] S. Daikh, F. Z. Zeggai, A. Bellil, and A. Benyoucef, "Chemical polymerization, characterization and electrochemical studies of PANI/ZnO doped with hydrochloric acid and/or zinc chloride: Differences between the synthesized nanocomposites," Journal of Physics and Chemistry of Solids, vol. 121, pp. 78-84, Oct. 2018.

[22] A. K. M. A. Ullah et al., "Green synthesis of Bryophyllum pinnatum aqueous leaf extract mediated bio-molecule capped dilute ferromagnetic α-MnO2 nanoparticles," Materials Research Express, vol. 7, no. 1, p. 015088, Jan. 2020.

[23] A. Abdelkhalek and A. A. Al-Askar, “Green synthesized ZnO nanoparticles mediated by Mentha spicata extract induce plant systemic resistance against Tobacco Mosaic Virus,” Applied Sciences, vol. 10, no. 15, p. 5054, Jul. 2020.

[24] G. C. Psarras, “Conductivity and dielectric characterization of polymer nanocomposites,” Elsevier eBooks, pp. 31-69, Jan. 2010.

[25] Z. H. Mahmoud, R. A. Al-Bayati, and A. A. Khadom, “In situ polymerization of polyaniline/samarium oxide - anatase titanium dioxide (PANI/Sm2O3-TiO2) nanocomposite: Structure, thermal and dielectric constant supercapacitor application study,” Journal of Oleo Science, vol. 71, no. 2, pp. 311-319, Jan. 2022.

[26] A. H. Majeed et al., “A review on polyaniline: Synthesis, properties, nanocomposites, and electrochemical applications,” International Journal of Polymer Science, vol. 2022, pp. 1-19, Oct. 2022.

[27] R. M. Attia, N. M. Yousif, R. H. Helal, and N. M. Ali, “Fabricating electronic textile using nano MnO2/polyaniline composites for capacitor device,” Journal of Industrial Textiles, p. 152808371989676, Dec. 2019.

[28] S. Nandi, S. S. Kerur, and S. Dhanalakshmi, “Electrical and dielectric properties of polymer-metal hybrid nanocomposites - a short review,” Diffusion Foundations and Materials Applications, vol. 35, no. 35, pp. 1-13, Jun. 2024.

[29] H. R. El Bahi, M. Mahdi, and D. Mohamed, “Synthesis, characterization, optical, and electrical properties of polyvinyl alcohol/nano erbium oxide hybrid nanocomposites,” Journal of Inorganic and Organometallic Polymers and Materials, vol. 34, no. 12, pp. 6114-6127, Jul. 2024.

[30] A. S. Gadtya, S. Chakroborty, S. Moharana, S. Singh, H. Kaur, and I. A. Darwish, “Enhancement of dielectric and electrical properties of polyvinyl alcohol-NaNbO3-copper nanoparticle composite films,” Journal of Molecular Liquids, vol. 423, p. 127030, Jan. 2025.